

## Retrofitting RC beams with different FRP types under blast loads.

Mahmoud Samak<sup>1</sup>, Ehab Lotfy<sup>2</sup>, Manar A. Ahmed<sup>2</sup>, Erfan Abdel Latif<sup>2</sup>

<sup>1</sup>(Civil Engineering, El-Arish High Institute for Engineering and Technology, North Sinai, Egypt)

<sup>2</sup>(Civil Engineering, Faculty of Civil Engineering/ Suez Canal University, Ismailia, Egypt)

### Abstract:

The blast load is the dynamic load that an engineer may face during the design procedure. This paper used the ABAQUS program to simulate reinforced concrete (RC) beams retrofitted with BFRP, CFRP, and GFRP sheets subjected to blast loads. The experiment data is simulated in the ABAQUS program to validate the ABAQUS modeling, it was collected from a last experiment research. The deflection, reaction force, and damage mode of RC beams under blast loading are studied. The dimension models are 150 x 250 x 2500 mm. The characteristic compressive strength of concrete ( $f_{cu}$ ) is 25 MPa. The parametric studies of ABAQUS models are the standoff distance ( $D$ ), TNT weights, and FRP types. The results show that, RC beams are damaged in flexure-shear and flexure. the spallation area significantly affects scaled distance. The retrofitting with FRP sheets decreases the deflection and reaction force addition to enhance the resistance of beams to damage. It is observed that the GFRP sheets significant effect than the CFRP and BFRP sheets on the behavior of retrofitting RC beams under-blast loads.

**Key Word:** Blast load, Explosion waves, RC beams, ABAQUS, FRP sheets.

Date of Submission: 01-11-2023

Date of acceptance: 10-11-2023

### I. Introduction

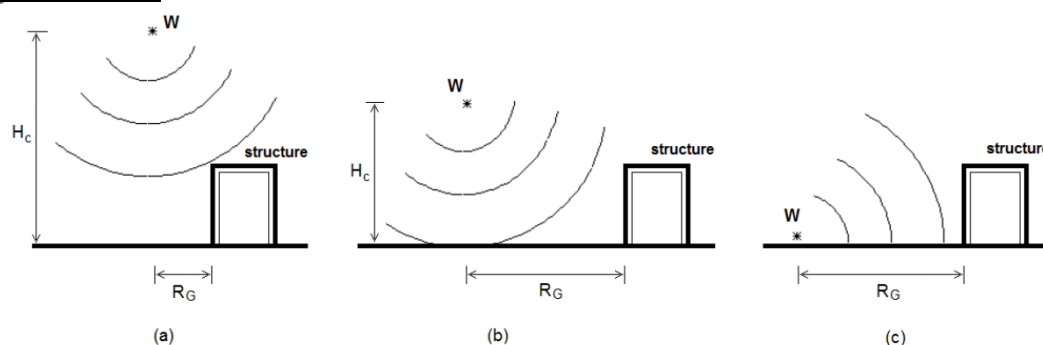
As presented in fig. 1, they can be illustrious in three main categories of explosion waves:

Free-air bursts: The explosive charge explodes in the atmosphere; the explosion waves impose directly onto the building without contact with the land.

Air bursts: The explosive charge is exploded in the atmosphere; the explosion waves are imposed onto the building after having contact first with the land; a Mach wave front is formed.

Surface bursts: The explosive charge explodes nearly at the land surface; the explosion waves direct contact with the land, and they spread hemispherical outwards and imposed onto the building.

$H_c$  is the height over ground,  $W$  explosion charge, and  $R_G$  is the horizontal distance between the explosive charge and the building. Related to each blast category is a typical blast loading of the building, this paper concentrated on the free air bursts.



**Figure 1:** Types of explosion waves; (a) Free-air bursts, (b) Air bursts, and (c) Surface bursts.

When the explosion wave reaches the touch base of a rigid body the reflected pressure is bigger than the incident peak pressure  $P_i$  as shown in fig. 2. The cause for this increase is ascribed to the character of the spread of the explosion wave through the air. While the wave moves, it travels through air atoms that strike with the surface upon influx. In an ideal linear-elastic case the atoms should be able to bounce back freely chief to a reflected pressure equivalent to the incident pressure, and thus the surface would undergo a doubling of the acting pressure. In a powerful explosion wave, which as a shock wave is a non-linear phenomenon, the reflection of these atoms is blocked by later air atoms that are moved there, thus causing lots greater reflected pressure values. In this case, the surface would undergo an acting pressure lot greater than the incident one. It is this reflected pressure to be utilized for design. Figure 2 shows the change between the incident and the reflected pressure on a large surface. As just observed, the reflected pressure can be numerous times bigger than the incident pressure, depending on the shape of the building, the style, size, weight, and distance of the explosive as well as the surface of other body between the explosion point and the building [1]. Figure 2 also represents a typical dynamic pressure time history, in which the change is that both incident and reflected pressures last only for a very quick time (commonly far less than one second), but the dynamic pressure may last for longer times (up to 2-3 seconds). The explosion wave spreads in the atmosphere with always reducing speed which is greater than the speed of sound. The air after the front of the explosion wave travels similarly along the matching path as the wind however with a smaller speed. These winds after the explosion wavefront are accountable for loading a surface for the whole period of the positive phase and for a small period afterward [2].

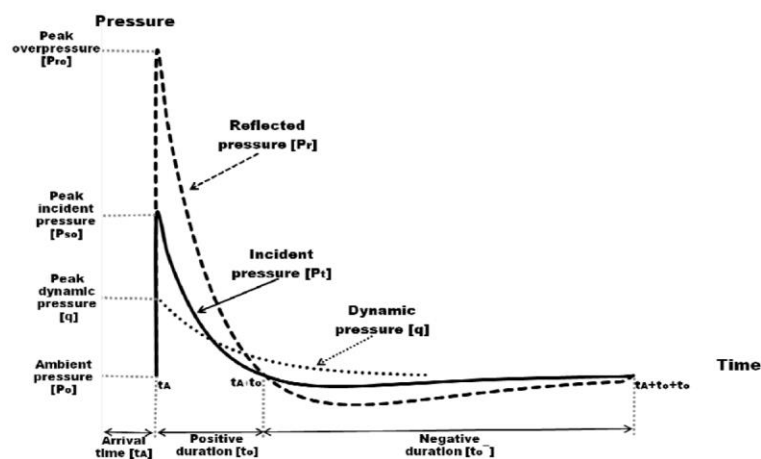


Figure 2: Reflected, incident, and dynamic pressure time histories.

Hopkinson-Cranz Scaling says that if any two bombs have equal scaled distances, they will give the same overpressure even if it has different weight and standoff distance[3].  $Z$  is the scaled distance ( $m/Kg^{1/3}$ ),  $D$  is the distance between the bomb and the building(meter), and  $W$  is the TNT weight (Kg).

$$Z = \frac{D}{\sqrt[3]{W}} \quad (1)$$

## II. Aim And Objectives

The research aim is to simulate the behavior of an RC beam under an explosion wave using ABAQUS. The objectives are to:

- 1) Show the response of the RC beam exposed to the blast waves.
- 2) Study the failure mode of the RC beam under blast waves.
- 3) Effect of FRP types on the behavior of retrofitting RC beams with under-blast loads.

## III. Numerical Analysis

The finite element modeling is used to study the effect of factors on the behavior of RC beams under explosion waves by the ABAQUS program. The last experimental research validates with ABAQUS models.

### Verification of the nonlinear finite element modeling

The experimental study was presented on RC beams under blast loading[4]. The dimensions of the beam were 100 x 100 x 1100 mm as shown in table 1. The reinforcement steel for all specimens was 6 mm. The stirrups

spacing was 60 mm. The compressive strength of concrete was 40.45 MPa. The yield and ultimate strength of reinforcement steel were 395 and 501 MPa respectively.

**Table 1:** Experimental program.

Model	Dimension (mm)	TNT mass (kg)	Standoff distance (m)	Scale distance (m/kg <sup>1/3</sup> )
B2-1	100x100x1100	0.36	0.4	0.57
B2-4		0.75	0.4	0.40

The experimental study was presented on RC beams under blast loading[5]. The dimensions of the beam were 220 x 300 x 2000 mm. The reinforcements of all these beams are with a diameter of 12 mm. The stirrups spacing was C8@80 mm and C8@ 150 mm. For a steel bar, the yield strength and the elastic modulus were 458 MPa and 193 GPa respectively. The concrete material grade was C40. The beam was simply supported with 100 mm hanging over at each edge. The TNT was over in the mid-span of the beam as shown in table 2.

**Table 2:** Blast protocol of concrete beams.

Model	Dimension (mm)	TNT mass (kg)	Standoff distance (m)	Scale distance (m/kg <sup>1/3</sup> )
S12-1-2	220x300x2000	1	0.50	0.5000
S12-2		2	0.65	0.5159
S12-3		3	0.65	0.4507

RC beams and beam-columns transversely wrapped with SRP tested under blast load[6]. Ten RC members were tested under change blast load. The dimensions were 150 x 150 x 2100 mm as follows in table 3. The longitudinal and tied reinforcement were with a diameter of 6mm. The spacing of the stirrups was 60mm. The compressive strength of concrete was 39.1 MPa. The yield and ultimate reinforcement strength were 500 MPa and 600 MPa respectively.

**Table 3:** Blast protocol of concrete beams.

Model	Dimension (mm)	C4 mass (kg)	TNT mass (kg)	Standoff distance (m)	Scale distance (m/kg <sup>1/3</sup> )
B1	150x150x2100	20	25.8	2	0.677
C1		15	19.35	2	0.745

The models were adjusted until an agreeable error was obtained. The numerical search was prepared on RC beams subjected to explosion waves using the ABAQUS program. The validation was comparing mid-span deflection. Table 4 shows the comparison of mid-span displacements between experimental and ABAQUS models. As shown the change between experimental and numerical analysis results is agreeable.

**Table 4:**Maximum deflection for experimental and finite element modeling analysis.

Ref.	Model	Max. deflection (mm)		Error (%)
		Experimental	ABAQUS	
[4]	B2-1	9	9.07	0.78
	B2-4	40	37.45	6.38
[5]	S12-1-2	3.31	3.12	8.76
	S12-2	4.89	5.06	9.29
	S12-3	11.14	11.06	0.72
[6]	B1	22	20.31	7.68
	C1	8	8.74	9.25

### Nonlinear finite element modeling

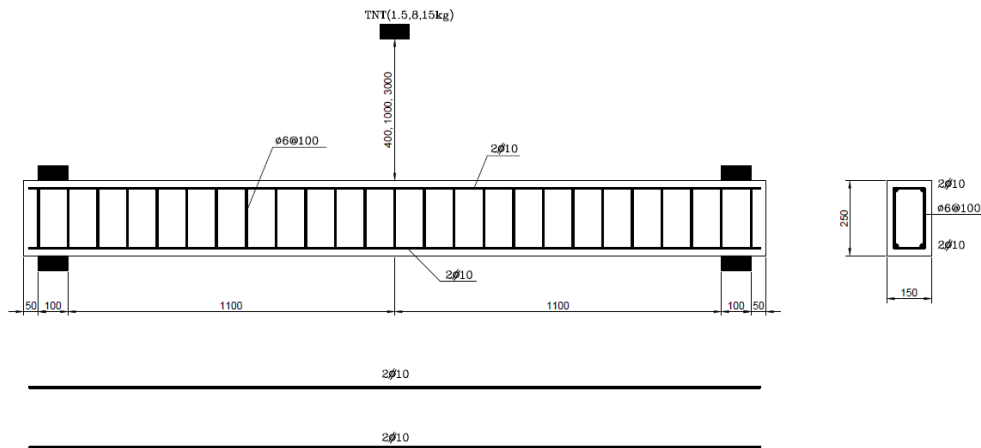
This thesis studies the behavior of RC beams subjected to blast load using ABAQUS. Beams with dimensions of 150 x 250 x 2500 mm were used in the numerical analysis. The characteristic compressive strength of concrete  $f_{cu}$  is 25 MPa. The diameter of longitudinal reinforcement and transverse reinforcement is 10 and 6 mm respectively. The spacing between stirrups is variable 100 mm. The blast loading used in the ABAQUS was placed over the center of the RC beam as shown in fig. 3. The yield and ultimate strength of the reinforcing steel 6 mm were 240 MPa and 350 MPa respectively, and the reinforcing steel 10 mm were 390 MPa and 560 MPa, respectively. The U total wrapped of FRP sheets is used to retrofit the RC beams as shown in fig. 4. Sika Wrap Hex-430G is an E-Glass fabric of 0.168 mm fiber thickness, 2500 MPa fiber tensile strength, and the modulus of elasticity was 72000 MPa. Sika Wrap Hex-300C is a Carbon fabric of 0.167 mm fiber thickness, 4000 MPa fiber tensile strength, and a modulus of elasticity of 230000 MPa and 1.7% tensile elongation. BFRP is a Basalt fabric

of 0.12 mm fiber thickness, 2100 MPa fiber tensile strength, a modulus of elasticity of 77900 MPa, and 2.1% tensile elongation. The tested parameters of this research are as follows in table 5:

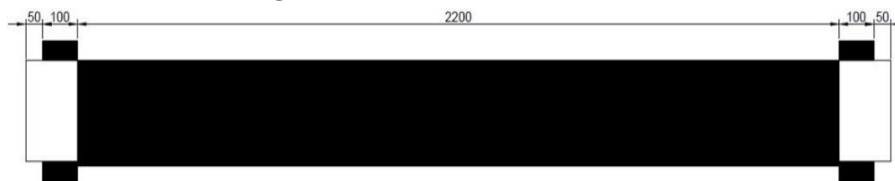
- 1) The TNT weights.
- 2) standoff distance D.
- 3) FRP types.

**Table 5:** Parametric study of ABAQUS models.

Parametric study		Symbols	Values
Z (m/kg <sup>1/3</sup> )	TNT (Kg)	T <sub>1</sub>	1.5
		T <sub>2</sub>	8
		T <sub>3</sub>	15
	Standoff distance (mm)	D <sub>1</sub>	400
		D <sub>2</sub>	1500
		D <sub>3</sub>	3000
FRP types		G	GFRP
		C	CFRP
		B	BFRP



**Figure 3:** Details of ABAQUS models.



**Figure 4:** Details total wrapped of retrofitting RC beam.

The ABAQUS program is applied to the analysis of RC beams. There are three main parts for modeling: the concrete body that is modeled using a solid element, steel reinforcement that is modeled as a rebar element, and FRP that is modeled as a shell element. The analysis step chosen was dynamic explicit. In finite elements, the concrete damage plasticity model (CDP) is used to model the behavior of concrete [7], [8]. For the reinforcing steel is considered as the elastic-plastic behavior. FRP was defined by using the elastic-plastic behavior with lamina type. The concrete and steel reinforcement geometry were modeled as solid deformable and wire deformable elements respectively. The concrete beam meshed as structural elements of 8 node hexahedral linear brick element (C3D8R) with a 20 mm mesh size while steel reinforcement was meshed with 2 node linear truss element (T3D2) with a 5 mm mesh size and FRP was meshed with 4 nodes doubly curved thin or thick shell element (S4R) with 20 mm mesh size. The constraint-embedded region option is modeled as an interaction between concrete and steel. The concrete is chosen as the host region and the steel reinforcement is the embedded region. The interaction between concrete and FRP is modeled using the constraint tie option, whereas the concrete and FRP are selected as the master surface and slave surface respectively. The blast load is described with the

Conventional Weapons Effects Program (CONWEP) interaction property. For the boundary condition, two ends of the beam are pinned[9].

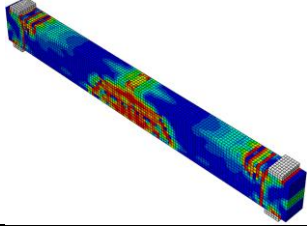
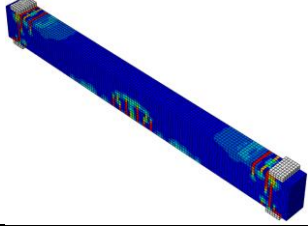

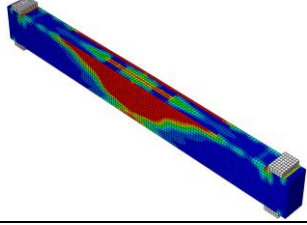
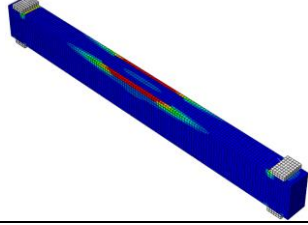
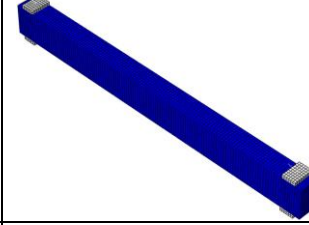
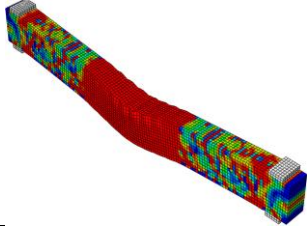
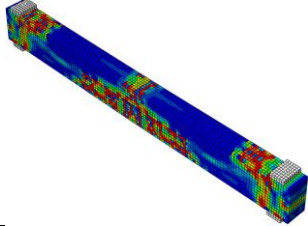
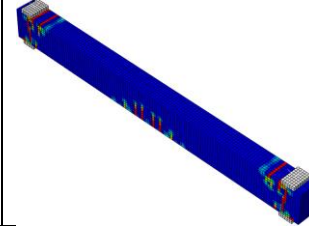
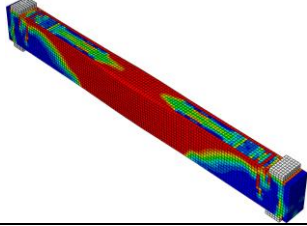
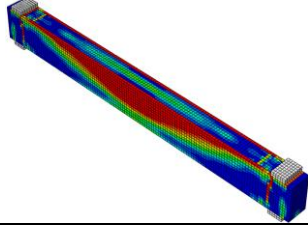

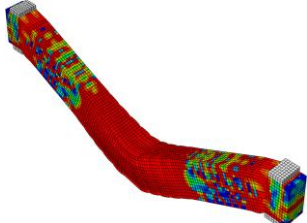
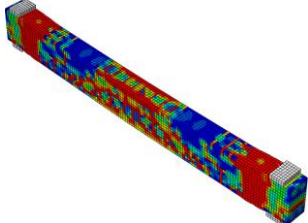
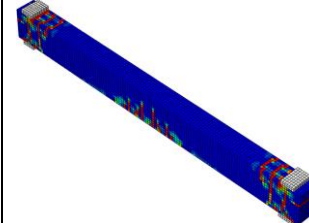
#### IV. Result

The simulations were run on thirty-six RC beams exposed to blast loading. The factors such as standoff distance, mass of TNT, and retrofitting technique of GFRP sheets have been studied. The deflection (Y), reaction forces (F), and damage mode against the last parameters are studied in this section.

##### Failure mode and cracks pattern

The failure states of the control and retrofitting RC beams with different FRP types subjected to blast load are shown in table 6. The RC beams showed mixed failure damage of both local damage and global flexural failure.

**Table 6:** Comparison of damage between control and retrofitting models in ABAQUS.

Models	T1D1	T1D2	T1D3
Control			
Retrofitting			
Models	T2D1	T2D2	T2D3
Control			
Retrofitting			
Models	T3D1	T3D2	T3D3
Control			

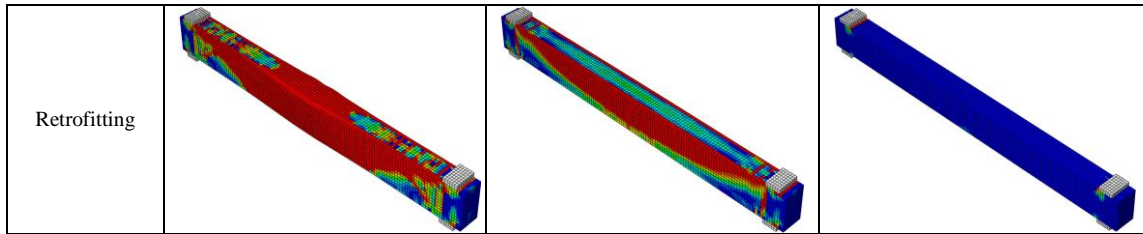


Table 6 shows that, there is almost no effect of the blast waves on the beam with a scaled distance of  $2.62 \text{ m/kg}^{1/3}$ . The maximum deflection was not exceeding  $0.49 \text{ mm}$ . Many cracks occurred at the center portion and near upper supports with a scaled distance range of  $0.87: 1.5 \text{ m/kg}^{1/3}$ . The maximum deflection range was  $1.8: 3 \text{ mm}$ . A part of the concrete at the top central beam was broken in addition to diagonal and flexural cracks developing from the lower edge and many cracks occurred near upper supports with scaled distance range  $0.35: 0.5 \text{ m/kg}^{1/3}$ . The maximum deflection range was  $6: 40 \text{ mm}$  respectively. The core concrete of the center portion completely failed with a scaled distance range of  $0.16: 0.2 \text{ m/kg}^{1/3}$ . The maximum deflection range was  $164: 450 \text{ mm}$ . The displacement and intensity of the failure region increased with the decrease in the scaled distance.

**Parametric study**

**Table 7:** Maximum deflection, reaction force, and damage mode of control and retrofitting ABAQUS models.

Models	$Y_{\max}$ (mm)	$F_{\max}$ (KN)	Damage mode	Models	$Y_{\max}$ (mm)	$F_{\max}$ (KN)	Damage mode
T1D1	5.02	356.53	Spalling	T1D1C	1.43	81.82	Spalling
T1D2	1.43	206.76	Cracks	T1D2C	0.26	45.85	Cracks
T1D3	0.29	54.99	Intact	T1D3C	0.08	7.12	Intact
T2D1	143.76	272.26	Damage	T2D1C	9.14	172.85	Damage
T2D2	10.38	436.78	Spalling	T2D2C	1.33	153.47	Spalling
T2D3	1.62	190.57	Cracks	T2D3C	0.28	50.72	Intact
T3D1	436.69	253.42	Damage	T3D1C	18.94	225.57	Damage
T3D2	33.4	186.76	Damage	T3D2C	3.19	236.04	Spalling
T3D3	2.85	302.14	Cracks	T3D3C	0.48	82.44	Intact
T1D1B	1.5	81	Spalling	T1D1G	1.33	75.55	Spalling
T1D2B	0.26	44.16	Cracks	T1D2G	0.24	37.49	Cracks
T1D3B	0.08	7.03	Intact	T1D3G	0.07	6.63	Intact
T2D1B	10.06	181.82	Damage	T2D1G	8.37	167.83	Damage
T2D2B	1.38	156.78	Spalling	T2D2G	1.12	133.89	Spalling
T2D3B	0.28	50.25	Intact	T2D3G	0.24	37.83	Intact
T3D1B	21.63	233.9	Damage	T3D1G	18	213	Damage
T3D2B	3.17	242.06	Spalling	T3D2G	2.15	226.55	Spalling
T3D3B	0.49	82.16	Intact	T3D3G	0.41	73.14	Intact

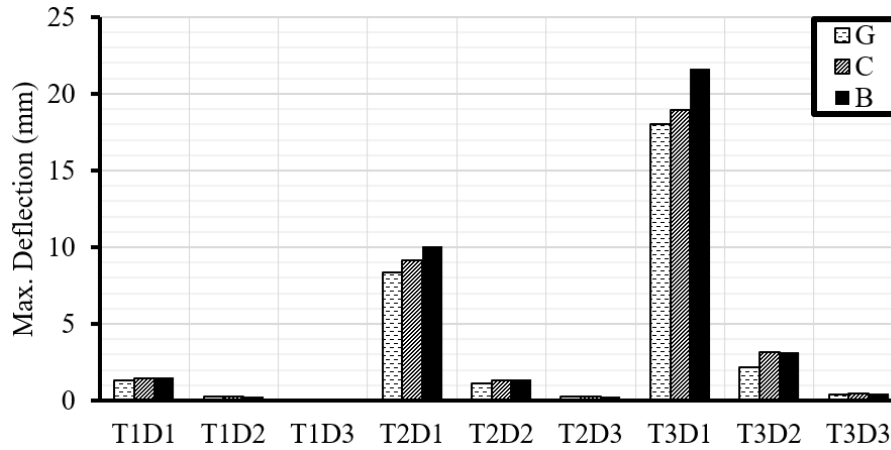


Figure 5: Max. deflection of retrofitted models with different FRP types.

In fig. 5, with different FRP types, the deflection decreases with GFRP than with CFRP and BFRP sheets with ratios that do not exceed 21 %. While with an increase in the TNT weight for the same model, the deflection increase with ratio does exceed 450%. Additionally, with an increase in the standoff distance for the same model, the deflection decreases with a ratio of not less than 94 %. From the last results, the effect of GFRP is better than CFRP and BFRP sheets in the deflection. While it shows a significant effect with different scaled distances in the deflection.

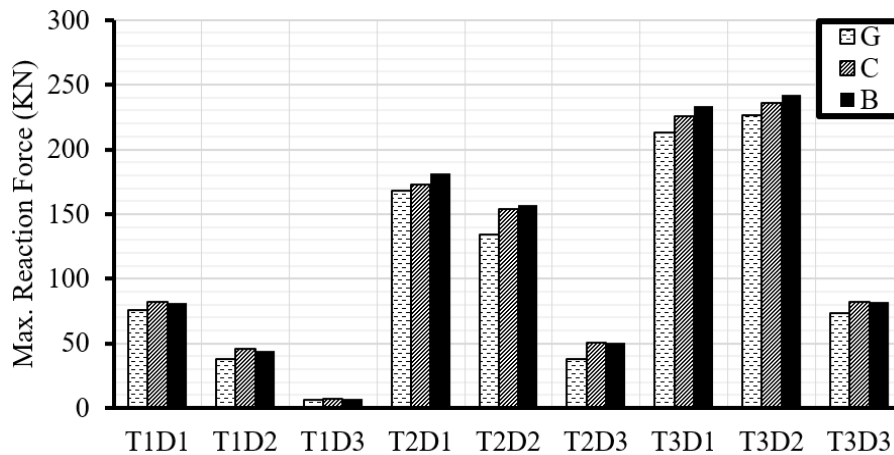


Figure 6: Max. reaction force of retrofitted models with different FRP types.

In fig. 6, with different FRP types, the reaction force decreases with GFRP than with CFRP and BFRP sheets with ratios that do not exceed 34 %. While with an increase in the TNT weight for the same model, the reaction force increase with ratio does exceed 70%. Additionally, with an increase in the standoff distance for the same model, the deflection decreases with a ratio of not less than 40 %. From the last results, the effect of GFRP is better than CFRP and BFRP sheets in the reaction load. While it shows a significant effect with different scaled distances in the reaction load.

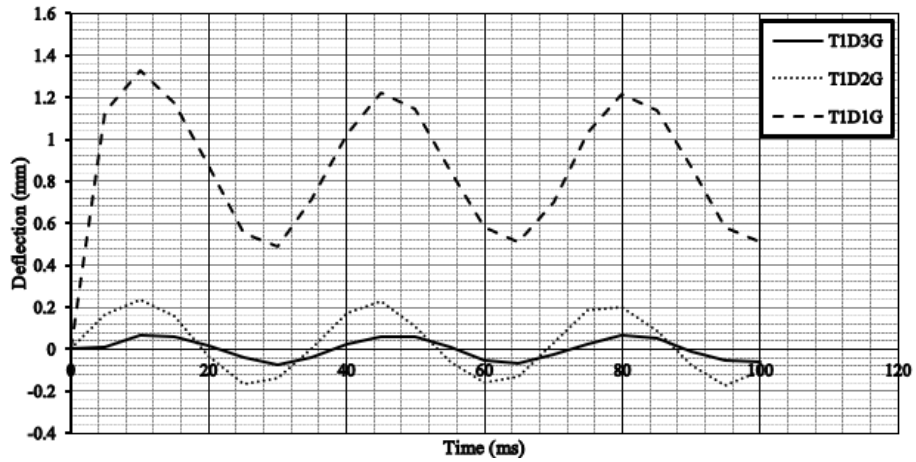


Figure 7: Deflection-time curve for T1G models with different standoff distances.

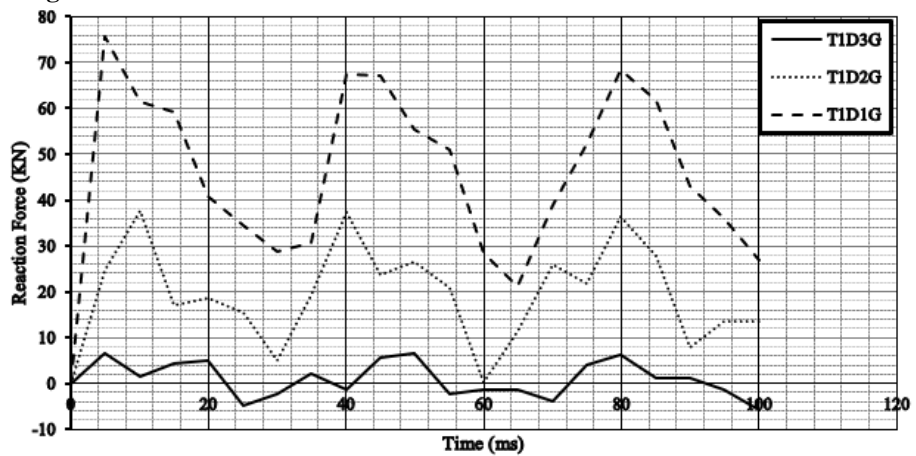


Figure 8: Reaction force-time curve for T1G models with different standoff distances.

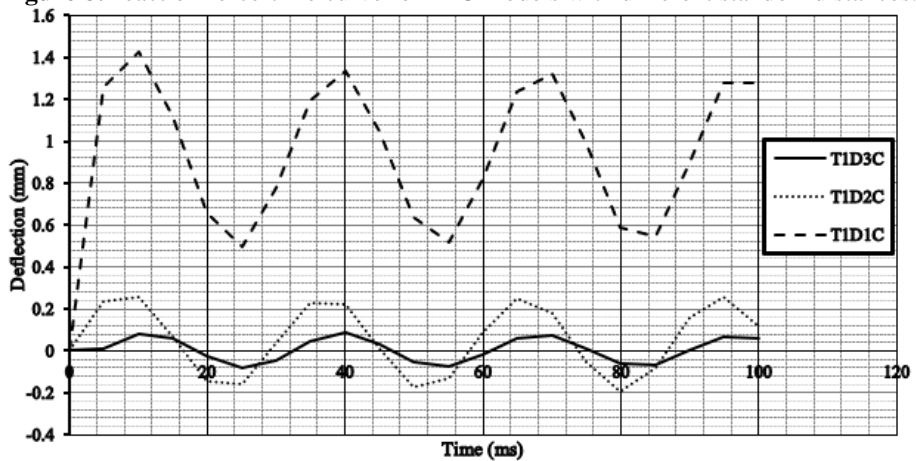


Figure 9: Deflection-time curve for T1C models with different standoff distances.



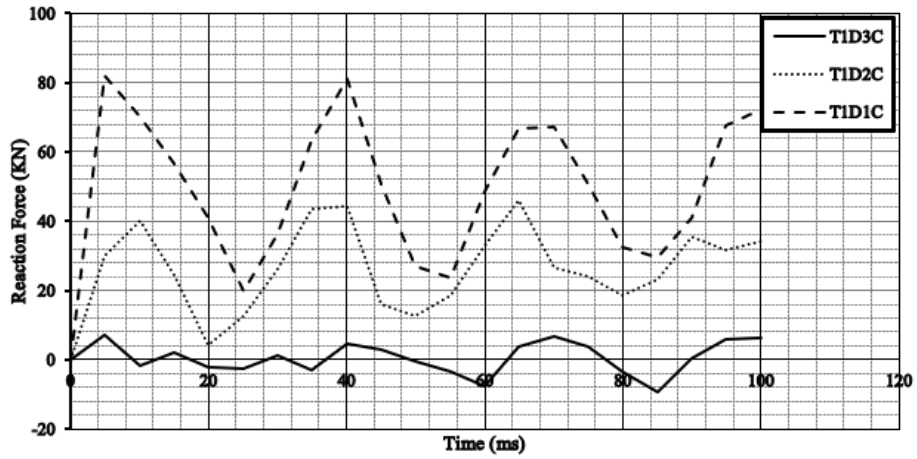


Figure 10: Reaction force-time curve for T1C models with different standoff distances.

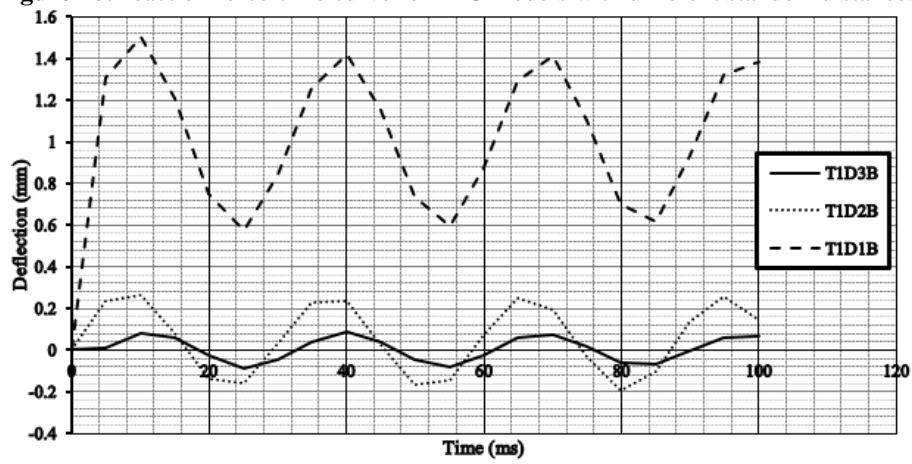


Figure 11: Deflection-time curve for T1B models with different standoff distances.

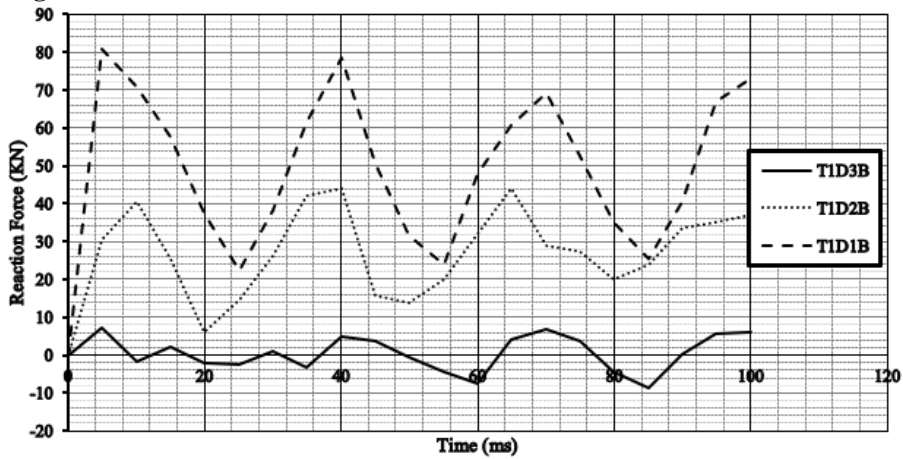
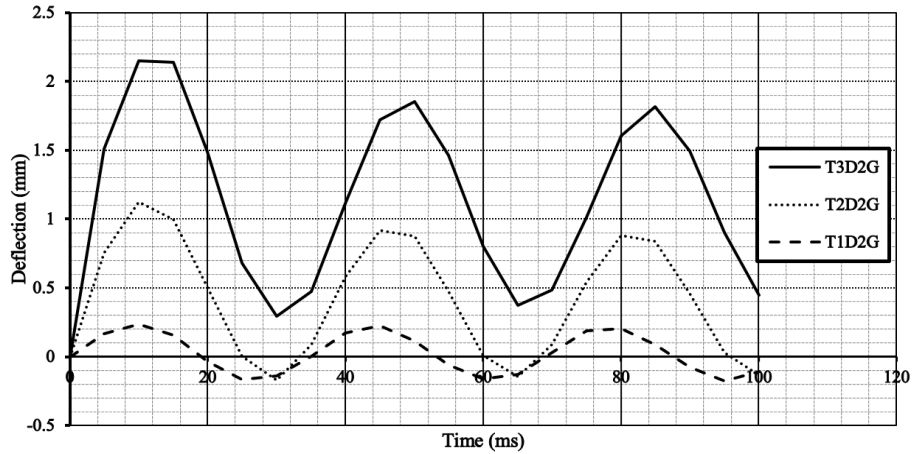
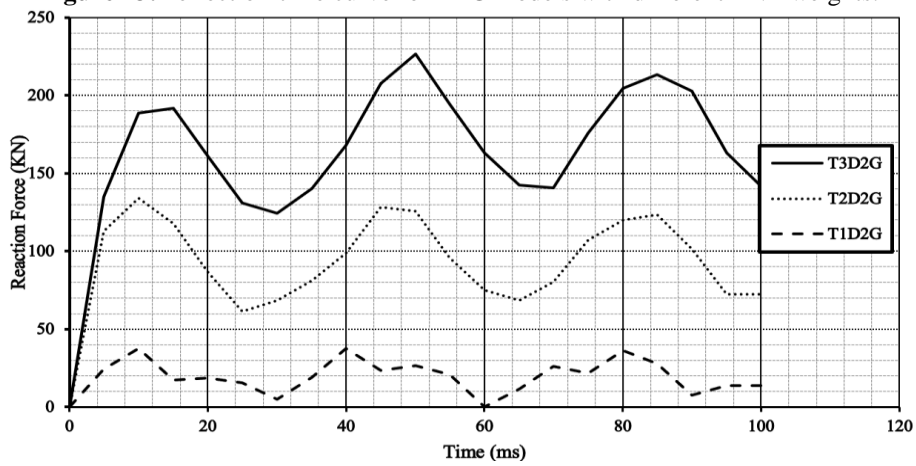


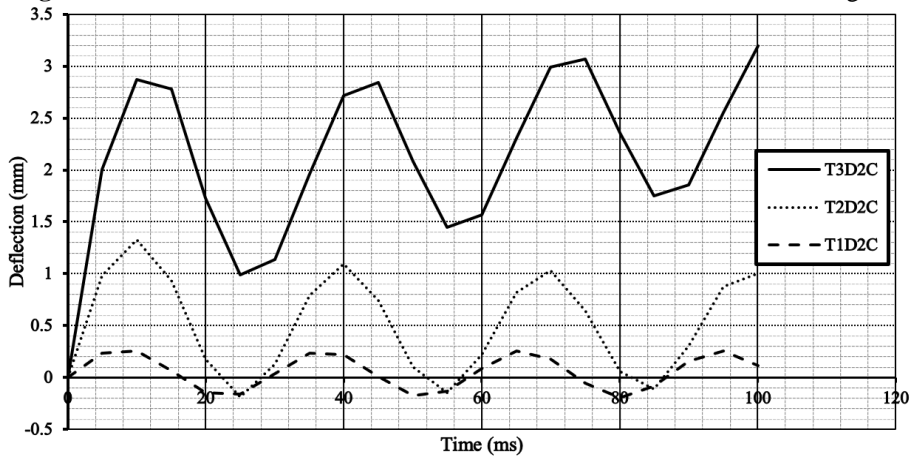
Figure 12: Reaction force-time curve for T1B models with different standoff distances.



**Figure 13:** Deflection-time curve for D2G models with different TNT weights.



**Figure 14:** Reaction force-time curve for D2G models with different TNT weights.



**Figure 15:** Deflection-time curve for D2C models with different TNT weights.

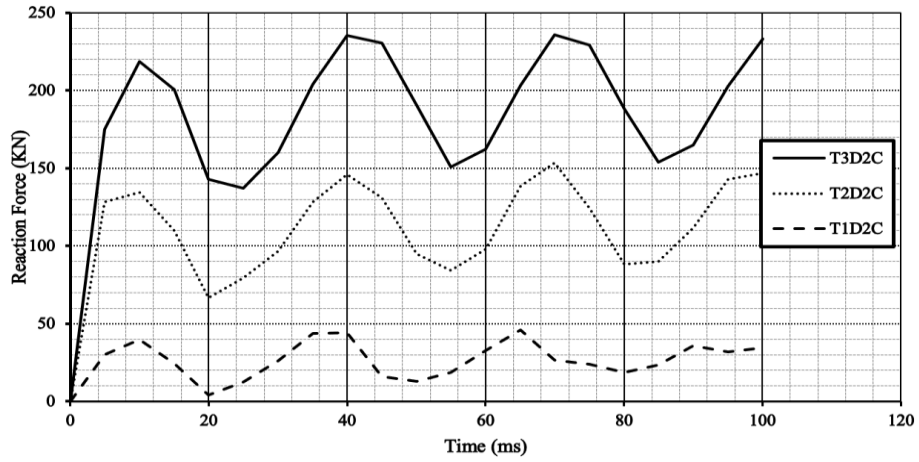


Figure 16: Reaction force-time curve for D2C models with different TNT weights.

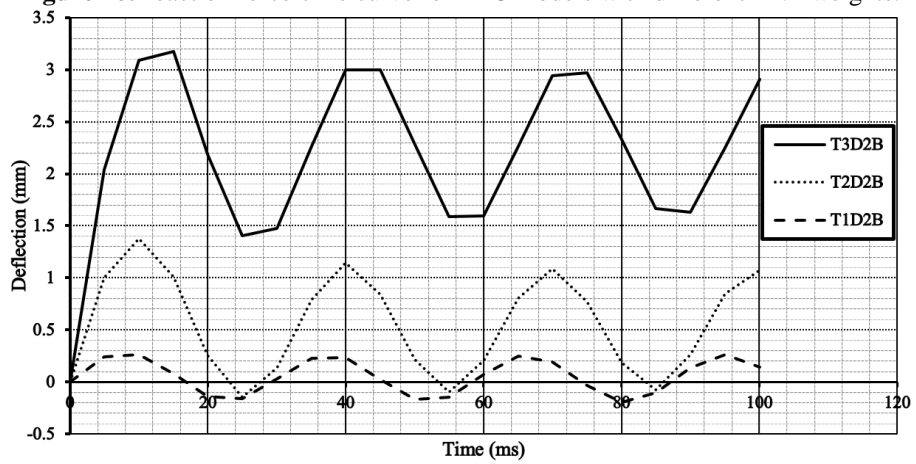


Figure 17: Deflection-time curve for D2B models with different TNT weights.

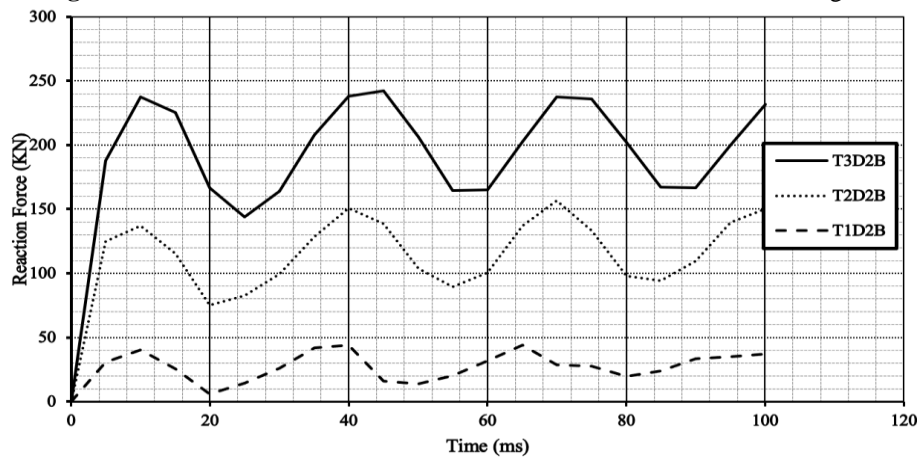


Figure 18: Reaction force-time curve for D2B models with different TNT weights.

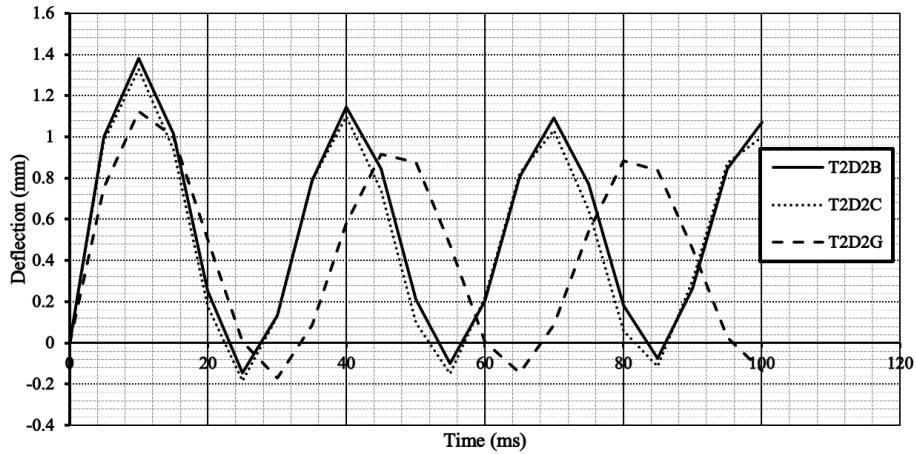


Figure 19: Deflection-time curve for T2D2 models with different FRP types.

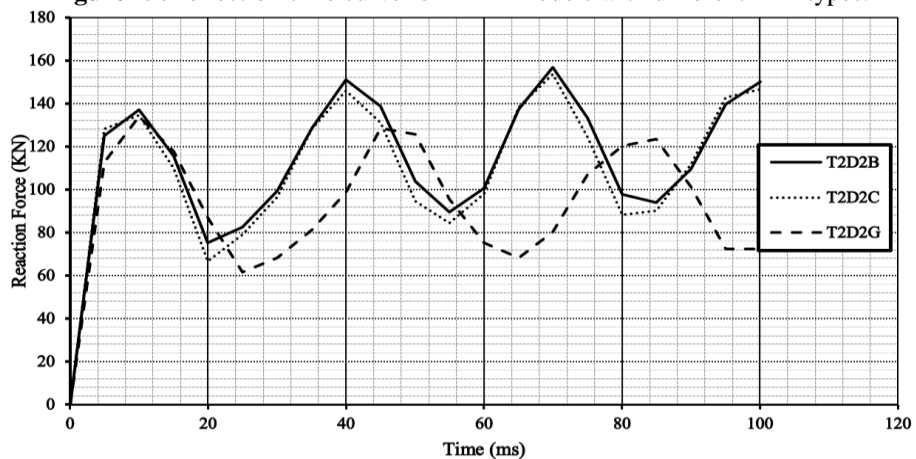


Figure 20: Reaction force-time curve for T2D2 models with different FRP types.

## V. Discussion

From fig. 5 and 6, the effect of GFRP is better than CFRP and BFRP sheets in the reaction force and deflection. Additionally, the scaled distance has a significant effect on the deflection and reaction force. In fig. 7-12, illustrates the behavior of most models with an increase in the TNT weight, the reaction force, and deflection significantly increase. In fig. 13-18, illustrates the behavior of most models with an increase in the standoff distance, the reaction force and deflection significantly decrease. Figures 19 and 20, illustrate the behavior of all retrofitting models with different FRP types, the reaction force and deflection significantly decrease with all FRP types. Additionally, GFRP can resist the explosive shock than CFRP and BFRP sheets, which are illustrated by streamlining the curves.

## VI. Conclusion

This study proposed an ABAQUS model to study the behavior of RC beams subjected to explosion waves under parameters of TNT weights, standoff distance, and FRP types. The numerical modeling results are compared with the previous research. The numerical results show the deflection, reaction force, and damage mode for RC beams. The conclusions are:

1. The finite element ABAQUS program agrees to predict the behavior of RC beams subjected to blast loads.
2. For different Z, lower scaled distance is more significant than high scaled distance in deflection and reaction forces.
3. The retrofitting models with different FRP types significantly decrease both the deflection and reaction force than the control models and enhance the damage mode as well.

4. It is noticed that GFRP sheets are more ductile than CFRP and BFRP sheets, so the deflection and the reaction force are decreased with the GFRP sheets than with CFRP and BFRP sheets.
5. For retrofitting techniques, GFRP sheets can resist explosive shock more than CFRP and BFRP sheets, which are illustrated by streamlining the curves.

### References

- [1] V. Karlos, G. Solomos, and B. Viacoz, *Calculation of blast loads for application to structural components*. Luxembourg: Publications Office of the European Union, 2013.
- [2] B. Samali, G. McKenzie, C. Zhang, and E. Ancich, "Review of the basics of state of the art of blast loading," *Asian J. Civ. Eng.*, vol. 19, no. 7, pp. 775–791, Nov. 2018, doi: 10.1007/s42107-018-0063-y.
- [3] Unified Facilities Criteria (UFC) 3-340-02, *structures to resist the effects of accidental explosions*. U.S. Department of Defense (DoD), 2008. [Online]. Available: <http://dod.wbdg.org/>.
- [4] D. Zhang *et al.*, "Experimental study on scaling of RC beams under close-in blast loading," *Eng. Fail. Anal.*, vol. 33, pp. 497–504, Oct. 2013, doi: 10.1016/j.engfailanal.2013.06.020.
- [5] S. Liu *et al.*, "Blast responses of concrete beams reinforced with GFRP bars: Experimental research and equivalent static analysis," *Compos. Struct.*, vol. 226, Oct. 2019, doi: 10.1016/j.compstruct.2019.111271.
- [6] M. Carriere, P. J. Heffernan, R. G. Wight, and A. Braimah, "Behaviour of steel reinforced polymer (SRP) strengthened RC members under blast load," *Can. J. Civ. Eng.*, vol. 36, no. 8, pp. 1356–1365, Aug. 2009, doi: 10.1139/L09-053.
- [7] S. V Chaudhari and M. A. Chakrabarti, "Modeling of concrete for nonlinear analysis Using Finite Element Code ABAQUS," 2012.
- [8] A. Jahami, Y. Tamsah, and J. Khatib, "The efficiency of using CFRP as a strengthening technique for reinforced concrete beams subjected to blast loading," *Int. J. Adv. Struct. Eng.*, vol. 11, no. 4, pp. 411–420, Dec. 2019, doi: 10.1007/s40091-019-00242-w.
- [9] "Abaqus/CAE User's Manual Abaqus 6.17 Abaqus/CAE User's Manual."